Active Center Cleft Residues of Pokeweed Antiviral Protein Mediate Its High-Affinity Binding to the Ribosomal Protein L3[†]

Francis Rajamohan,*[,‡,§] Zahide Ozer,[||] Chen Mao,[⊥] and Fatih M. Uckun*[,‡,#]

Biotherapy Program, Parker Hughes Cancer Center, and Departments of Protein Engineering, Biochemistry, Structural Biology, and Virology, Parker Hughes Institute, St. Paul, Minnesota 55113

Received December 15, 2000; Revised Manuscript Received June 5, 2001

ABSTRACT: Pokeweed antiviral protein (PAP) is a ribosome-inactivating protein (RIP) which catalytically cleaves a specific adenine base from the highly conserved α-sarcin/ricin loop (SRL) of the large ribosomal RNA and thereby inhibits the protein synthesis. The ribosomal protein L3, a highly conserved protein located at the peptidyltransferase center of the ribosomes, is involved in binding of PAP to ribosomes and subsequent depurination of the SRL. We have recently discovered that recombinant PAP mutants with alanine substitution of the active center cleft residues ^{69}NN^{70} (FLP-4) and ^{90}FND^{92} (FLP-7) that are not directly involved in the catalytic depurination at the active site exhibit >150-fold reduced ribosome inhibitory activity [(2000) *J. Biol. Chem. 275, 3382*−*3390*]. We hypothesized that the partially exposed half of the active site cleft could be the potential docking site for the L3 molecule. Our modeling studies presented herein indicated that PAP residues 90−96, 69−70, and 118−120 potentially interact with L3. Therefore, mutations of these residues were predicted to result in destabilization of interactions with rRNA and lead to a lower binding affinity with L3. In the present structure−function relationship study, coimmunoprecipitation assays with an in vitro synthesized yeast ribosomal protein L3 suggested that these mutant PAP proteins poorly interact with L3. The binding affinities of the mutant PAP proteins for ribosomes and recombinant L3 protein were calculated from rate constants and analysis of binding using surface plasmon resonance biosensor technology. Here, we show that, compared to wild-type PAP, FLP-4/^{69}AA^{70} and FLP-7/^{90}AAA^{92} exhibit significantly impaired affinity for ribosomes and L3 protein, which may account for their inability to efficiently inactivate ribosomes. By comparison, recombinant PAP mutants with alanine substitutions of residues ^{28}KD^{29} and ^{111}SR^{112} that are distant from the active center cleft showed normal binding affinity to ribosomes and L3 protein. The single amino acid mutants of PAP with alanine substitution of the active center cleft residues N69 (FLP-20), F90 (FLP-21), N91 (FLP-22), or D92 (FLP-23) also showed reduced ribosome binding as well as reduced L3 binding, further confirming the importance of the active center cleft for the PAP−ribosome and PAP−L3 interactions. The experimental findings presented in this report provide unprecedented evidence that the active center cleft of PAP is important for its in vitro binding to ribosomes via the L3 protein.

Pokeweed antiviral protein (PAP)[1] is a naturally occurring type I ribosome-inactivating protein (RIP) isolated from the leaves of the pokeweed plant, *Phytolacca americana* (*1*, *2*). The therapeutic potential of PAP as a ribosome inhibitory anticancer agent has gained considerable interest in recent years due to the clinical use of native PAP as the active moiety of immunoconjugates against cancer (*3*−*6*). PAP exhibits a highly specific RNA *N*-glycosidase activity that cleaves the glycosidic bond of a single adenine base (A^{4324} of the tetraloop sequence GAGA) that is located in the highly conserved "α-sarcin/ricin loop" (SRL) of the large ribosomal RNA (rRNA) species in eukaryotic (28S rRNA) and prokaryotic (23S rRNA) ribosomes (*7*, *8*). This catalytic depurination of the SRL by PAP results in irreversible inhibition of protein synthesis at the translocation step by impairing the elongation factor (EF) 1 dependent binding of aminoacyl-tRNA as well as the GTP-dependent binding of EF-2 to the affected ribosome (*3*, *9*−*11*).

Endo and Tsurugi (*8*) demonstrated that the ribosome inhibitory protein ricin-A chain is capable of deadenylating rat liver ribosomes with a K_{cat} value nearly 10^5-fold greater than that measured using naked 28S rRNA. The highly conserved catalytic site residues of the RIPs exhibit virtually the same level of depurinating activity for naked 28S rRNA derived from different species. However, these same RIPs differ in their depurinating activity against intact ribosomes isolated from different species (*7*, *12*). These observations imply an important role for ribosomal elements in RIP−rRNA interactions. A recent study by Hudak et al. (*13*)

[†] This work was supported by the Defense Advanced Research Projects Agency under Grant N65236-99-1-5422 (awarded to F.M.U.).

* To whom correspondence should be addressed: Parker Hughes Institute, 2657 Patton Road, Roseville, MN 55113. Phone: (651) 628-9988. Fax: (651) 697-1042. E-mail: frajamohan@ih.org; fatih_uckun@ih.org.

[‡] Biotherapy Program, Parker Hughes Cancer Center.

[§] Department of Protein Engineering, Parker Hughes Institute.

[||] Department of Biochemistry, Parker Hughes Institute.

[⊥] Department of Structural Biology, Parker Hughes Institute.

[#] Department of Virology, Parker Hughes Institute.

[1] Abbreviations: PAP, pokeweed antiviral protein; SRL, α-sarcin/ricin loop; EF, elongation factor; RIP, ribosome-inactivating protein; rRNA, ribosomal RNA; MBP, maltose binding protein; IPTG, isopropyl thiogalactoside; HM, *Haloarcula marismortui*.

10.1021/bi002851p CCC: $20.00
Published on Web 07/12/2001

indicated that the ribosomal protein L3, a highly conserved protein located at the peptidyltransferase center of the ribosomes, is involved in the binding of PAP to ribosomes and subsequent depurination of the SRL. Notably, PAP failed to depurinate ribosomes in yeast cells expressing a mutant L3 protein (*13*), prompting the hypothesis that the interaction of PAP with L3 is essential for its ability to bind to and inactivate ribosomes by depurination. Furthermore, footprinting studies of *Escherichia coli* 23S rRNA studies showed that L3, together with L6, has protected the SRL, suggesting that the protein L3 is located in close proximity to the SRL (*14*).

We have recently discovered that recombinant PAP mutants with alanine substitutions of the active center cleft residues ^{69}NN^{70} (FLP-4) and ^{90}FND^{92} (FLP-7) that are not directly involved in the catalytic depurination at the active site exhibit >150-fold reduced ribosome inhibitory activity (*15*). We hypothesized that the partially exposed half of the active site cleft could be the potential docking site for the L3 molecule. Our modeling studies indicated that PAP residues 90−96, 69−70, and 118−120 potentially interact with L3. The active center cleft residues Asn^{69}, Asn^{70}, and Asp^{92} as well as the active site residue Arg^{122}, which is not directly involved in the catalytic depurination of rRNA, promote specific interactions with the phosphate backbone of the target SRL of rRNA. On the other hand, these residues are on the protein surface, and all but residue 122 potentially interact with L3 in our model. Therefore, mutations of these residues were predicted to result in destabilization of interactions with rRNA and lead to a lower binding affinity with L3 (except 122). Coimmunoprecipitation assays with an in vitro synthesized yeast ribosomal protein L3 suggested that these active center cleft mutants of PAP poorly interact with L3. The binding affinities of the mutant PAP proteins for ribosomes and recombinant L3 protein were calculated from rate constants and analysis of binding using surface plasmon resonance (SPR) biosensor technology. Here, we show that, compared to wild-type PAP, FLP-4/^{69}AA^{70} and FLP-7/^{90}AAA^{92} exhibit significantly impaired affinity for ribosomes and L3 protein, providing a cogent explanation for their inability to efficiently inactivate ribosomes. The single amino acid mutants of PAP with alanine substitution of the active center cleft residues N69 (FLP-20), F90 (FLP-21), N91 (FLP-22), or D92 (FLP-23) also showed reduced L3 binding. By comparison, recombinant PAP mutants with alanine substitutions of residues ^{28}KD^{29} and ^{111}SR^{112} that are distant from the active center cleft showed normal binding affinity to ribosomes and L3 protein. The experimental findings presented herein provide unprecedented evidence that the active center cleft of PAP is important for its in vitro binding to ribosomes via the L3 protein.

EXPERIMENTAL PROCEDURES

Molecular Modeling. The molecular model of the PAP−rRNA stem loop complex was derived from the 2.4 Å crystal structure of a large ribosomal subunit from *Haloarcula marismortui* (HM) (Protein Data Bank access code 1FFK) (*16*) and the crystal structure of the PAP−nucleotide complex (access code 1pag). This model represents a refinement of our recently published model of the PAP−rRNA stem loop complex (*15*). First, we superimposed the HM ribosome structure with the stem loop structure in our previous PAP−RNA complex model. The conformation of rRNA was adjusted near the adenine A2697 (A2660 in *E. coli*) of the GAGA tetraloop, and the rest of the PAP molecule was left unchanged. The adenosine was manually adjusted by a 38° rotation at the C5′ position and a 5.4 Å translation of the adenine ring. The model was used to perform fixed docking using the Docking module in InsightII employing the CVFF and a Monte Carlo strategy in the Affinity program (InsightII User Guide 1991, MSI, San Diego, CA). The parameters used in this docking included searching for five unique structures, with 1000 minimization steps for each structure, energy range 10.0 kcal/mol, maximum translation of the ligand of 3.0 Å, maximum rotation of the ligand of 10°, and an energy tolerance of 1500 kcal/mol. During the minimization steps of the docking procedure, only the tetraloop and the active site residues of PAP were allowed to be flexible, whereas the rest of rRNA and PAP remained fixed. The best molecular position was chosen on the basis of the best Ludi score which included the contribution of the loss of translational and rotational entropy of the RNA fragment, the number of hydrogen bonds, the hydrogen bond geometry, and contributions from ionic and lipophilic interactions to the binding energy. The refined structure was then analyzed in CHAIN (*17*). Finally, we examined the potential docking site for the L3 molecule. On the basis of the HM crystal structure, a rational choice for a binding location for PAP would be on the outer surface near residues 65 and 350, in a region that does not interact with rRNA and is closest to the SRL region. Therefore, the rRNA region containing SRL between 2684 and 2704 (2647 and 2667, respectively, in *E. coli*) and the PAP molecule were docked as a rigid body near the aforementioned region of L3. This was accomplished using the Docking module within the InsightII program in a similar manner as for the docking of rRNA to PAP.

Construction of Mutants. The recombinant wild-type PAP construct (pBS-PAP) was obtained by subcloning the *PAP-I* gene (amino acids 22−313) at the *Bam*HI and *Hin*dIII sites of the *E. coli* expression vector, pBluescript SK$^-$ (Stratagene, La Jolla, CA). PAP mutants were constructed using site-directed mutagenesis techniques as described previously (*15*).

Expression and Purification of Mutants. Wild-type and mutant recombinant PAP proteins were expressed in *E. coli* MV1190 as inclusion bodies, isolated, solubilized, and refolded, as described previously (*18*). The refolded proteins were analyzed by SDS−12% polyacrylamide gel electrophoresis (PAGE). Protein concentrations were determined from the gel using bovine serum albumin (BSA) as a standard.

Immunoblot Analysis of PAP Mutants. One microgram of the protein samples was resolved on a SDS−12% PAGE gel and transferred onto a poly(vinylidene difluoride) (PVDF) membrane (Roche Molecular Biochemicals, Indianapolis, IN) using the Bio-Rad trans-blot apparatus, as described previously (*18*). The membrane was immunoblotted using rabbit anti-PAP serum (1:2000 dilution) and horseradish peroxidase conjugated goat anti-rabbit IgG (1:1000 dilution) as the primary and secondary antibodies, respectively. The blot was developed using 3,3′-diaminobenzidine (Sigma) as the colorimetric indicator for peroxidase activity.

In Vitro RNA Transcription and Radiolabeling of the L3 Protein. A plasmid containing the cDNA (pJD166.trp) that

encodes the *Saccharomycis cerevisiae* ribosomal protein L3, wild type, was a kind gift from Dr. Jonathan D. Dinman, University of Medicine and Dentistry of New Jersey. Radiolabeled L3 protein was synthesized by a linked transcription−translation system (TNT T3-coupled reticulocyte lysate system, Promega) according to the manufacturer's instructions (Promega). The translation products were resolved on SDS−10% PAGE; gels were dried and autoradiographed.

Coimmunoprecipitation. The mouse anti-L3 monoclonal antibody was a kind gift from Dr. Jonathan R. Warner, Department of Cell Biology, Albert Einstein College of Medicine, Bronx, NY. The in vitro synthesized L3 protein (8×10^4 cpm) was incubated with 1 mg of wild-type or mutant PAP proteins in 50 mL (final volume) of binding buffer (10 mM K_2HPO_4, 5 mM NaCl, pH 8.0) at 30 °C for 30 min. The PAP−L3 complex was coimmunoprecipitated by adding 5 μL of the mouse anti-L3 monoclonal antibody (1:500 dilution). After 60 min of incubation at 30 °C, the PAP−L3−antibody complex was precipitated by addition of 50 mL of protein A−Sepharose beads that had been pretreated with rabbit anti-mouse IgG (20 μL/mL beads) and the incubation continued for another 1 h at 4 °C. The beads were washed three times with phosphate-buffered saline containing 0.1% Triton X-100, and the proteins were eluted from the Sepharose beads with SDS sample buffer. The proteins were separated through SDS−12% PAGE, transferred to a PVDF membrane, and probed with the polyclonal rabbit anti-PAP antibody (1:2000 dilution) and horseradish peroxidase conjugated goat anti-rabbit IgG (1:1000 dilution) as the primary and secondary antibodies, respectively. The blot was developed using 3,3′-diaminobenzidine (Sigma) as the colorimetric indicator for peroxidase activity. The dried membrane was also exposed to autoradiography to estimate the amounts of L3 protein.

Preparation of Ribosomes and Binding to PAP Mutants. Ribosomes were isolated from rabbit reticulocyte-rich whole blood (Pel-Freez, Rogers, AR), as described previously (*19*). Ribosome binding assays were carried out by incubating 5 μg samples of ribosome isolates with 1 μg of wild-type or mutant PAP proteins in 50 μL of TKM buffer (25 mM Tris-HCl, pH 8.0, 25 mM KCl, 5 mM $MgCl_2$) for 30 min at 30 °C. The ribosome−PAP complexes were separated by ultracentrifugation (90 000 rpm for 30 min), and the pellet was washed three times with 100 μL of HEPES−T buffer (0.1% Tween-20, 10 mM HEPES, pH 8) in order to remove the unbound PAP. The proteins were solubilized with SDS sample buffer, separated by SDS−12% polyacrylamide gel electrophoresis (PAGE), transferred to a PVDF membrane, and probed with the polyclonal antibody to PAP.

Expression and Purification of Recombinant L3 Protein in E. coli. The plasmid containing the cDNA (pJD166.trp) that encodes the *S. cerevisiae* wild-type ribosomal protein L3 was subcloned into the fusion vector, pMAL-c2 (New England Biolabs Inc., Beverly, MA), downstream from the *malE* gene, which encodes the maltose binding protein (MBP). The resulting construct, pMAL-L3, was transformed into *E. coli* cells, and the expression of the MBP−L3 fusion protein was induced by the addition of IPTG (1 mM final concentration). The L3 fusion protein was purified by binding to an amylose affinity purification column according to the manufacturer's instructions (New England Biolabs). The purified MBP−L3 fusion protein was analyzed by SDS−10% PAGE.

Expression and Purification of Recombinant L3 Protein in a Baculovirus Expression System. The *L3* gene in plasmid pJD166.trp was amplified by polymerase chain reaction (PCR) using the *Nco*I site-containing 5′-primer, 5′-AATTATCCATGGCTCACAGAAAGTACG-3′, and the *Eco*RI site-containing 3′-primer, 5′-AATTATGAATTCTTATTACAAGTCCTTCTTCAAAGTACC-3′. PCR was performed in 25 cycles with a Ericomp, DeltaCycler II, DNA Thermocycler system using a Gene Amp kit (Takara Shuzo Co., Ltd.) according to the procedure recommended by the supplier. After digestion of the PCR fragment with *Nco*I and *Eco*RI, the 1170 base pair fragment product was cloned into the pFastBac HTb His-tagged vector. The final construct, pFas-L3, was expressed in SF9 cells using the Bac-To-Bac baculovirus expression system (Gibco Life Technologies) following the manufacturer's instructions (Gibco). The 6×His−L3 fusion protein was purified by using the nickel−NTA spin kit (Quiagen, Inc.), as described in Quiagen protocols.

Monitoring of Binding Interactions Using Surface Plasmon Resonance Technology. A BIAcore 2000 surface plasmon resonance-based biosensor system (Pharmacia Biosensor AB) was used to measure the kinetic parameters for the interactions between soluble recombinant PAP proteins (analytes) and the immobilized ribosomes or the ribosomal protein L3 (ligands). In ribosome binding assays, ribosomes were covalently linked to the dextran on the surface of research grade CM5 sensor chips via primary amino groups using the amine coupling kit from Pharmacia according to the manufacturer's instructions (Pharmacia). Thirty-five microliters of the ribosome isolate (10 μg/mL) in 10 mM sodium acetate, pH 5.5, was injected onto the surface at a flow rate of 5 μL/min. Typically, a 1200 RU resonance signal was obtained following this procedure. The protein samples were diluted in PBS buffer (1 mM KH_2PO_4, 10 mM Na_2HPO_4, 0.137 M NaCl, 2.7 mM KCl, 0.005% Tween P20, pH 7.4) to a final concentration of 50 nM before the injection. Samples were injected at 25 °C at a flow rate of 5 μL/min onto the sensor chip surface on which the ribosome had been immobilized or onto a control surface on which BSA had been immobilized. The binding surface was regenerated by washing with 2 M NaCl.

In binding assays using the MBP−L3 fusion protein, an anti-MBP antibody was covalently linked to the dextran on the surface of research grade CM5 sensor chips via primary amino groups using the amine coupling kit (Pharmacia). The CM5 chip was activated by injecting a mixture of *N*-hydroxysuccinimide and *N*-ethyl-*N*′-(3-dimethylaminopropyl)carbodiimide followed by 35 μL of the anti-MBP antibody (10 μg/mL) (New England Biolabs) in 10 mM sodium acetate, pH 5.0. Ethanolamine hydrochloride, pH 8.5, was injected to block unreacted *N*-hydroxysuccinimide esters (35 μL). The MBP−L3 fusion protein was captured by injecting 40 μL of the fusion protein (20 μg/mL) over the surface of the CM5 sensor chip, which was immobilized (amine coupling) with an anti-MBP antibody, at a flow rate of 5 μL/min in HBS−EP buffer (0.1 M HEPES, pH 7.4, 0.15 M NaCl, 3 mM EDTA, and 0.005% polysorbate 20). Typically, an average resonance (RU) signal of 1500 was obtained by following this procedure. Unoccupied sites were

blocked by injecting 30 μL of MBP (25 μg/mL) in HBS−EP buffer as above. The protein samples were diluted in HSEM buffer (10 mM HEPES, pH 8.0, 50 mM NaCl, 1 mM EDTA, 5 mM $MgCl_2$, and 0.005% polysorbate 20) to a final concentration of 50 nM before the injection. In a kinetic study, 30 μL of samples (150 nM) was injected at 25 °C at a flow rate of 8 μL/min onto the sensor chip surface on which the MBP−L3 fusion protein has been captured or onto a control surface on which MBP had been immobilized, using HBS−EP as the running buffer. Between samples, the binding surfaces were regenerated by a 3 min injection of 1 M NaCl and 50 mM NaOH solution at a flow rate of 10 μL/min. Each experiment was carried out at least twice on the same chip, and samples were injected in random order.

In binding assays using His-tagged recombinant L3 protein 6×His−L3 produced in the baculovirus expression system, the NTA sensor chip was saturated by injecting 20 μL of 500 mM $NiCl_2$ solution at a flow rate of 20 μL/min in NTA buffer (10 mM HEPES, 0.15 M NaCl, 50 mM EDTA, 0.005% Surfactant P20, pH 7.4). The 6×His−L3 protein was diluted in NTA buffer to a final concentration of 150 nM and was immobilized on the sensor chip by injecting 25 μL at a flow rate of 5 μL/min. Typically, an average resonance signal of 1000 RU was obtained by following this procedure. Between samples, the binding surface was regenerated by injecting 30 μL of regeneration buffer (10 mM HEPES, 0.15 M NaCl, 0.35 M EDTA, 0.005 Surfactant P20, pH 8.3) at a flow rate of 10 μL/min.

For the binding of L3 protein to the recombinant wild-type PAP, the N-terminus 6×His−PAP fusion protein was used. The 6×His−PAP protein was cloned, expressed, and purified from *E. coli* as described previously (*18*). The NTA sensor chip was activated by injecting 20 mL of 500 mM $NiCl_2$ in NTA buffer at a flow rate of 20 mL/min. The 6×His−PAP protein was diluted in NTA buffer to a final concentration of 150 nM and was immobilized on the sensor chip by injecting 20 μL at a flow rate of 5 μL/min, giving a change in RU value of 275. A 30 mL solution of MBP−L3 protein (25 nM) alone or after preincubation with 250 nM native or recombinant wild-type PAP in buffer (50 mM HEPES, 10 mM $MgCl_2$, 50 mM NaCl, pH 7.6) at room temperature for 1 h was then injected over immobilized 6×His−PAP at a flow rate of 8 μL/min. Between samples, the binding surface was regenerated by injecting 30 μL of regeneration buffer (10 mM HEPES, 0.15 M NaCl, 0.35 M EDTA, 0.005 Surfactant P20, pH 8.3) at a flow rate of 10 μL/min. As a control for nonspecific binding, a MBP−L3 sample solution was injected over the flow cell without the immobilized 6×His−PAP protein, and each control signal was subtracted to correct for a nonspecific binding.

The primary data were analyzed using the BIAevaluation software (Version 3.0) supplied with the instrument (Biacore, Inc.). To prepare the data for analysis, baselines were adjusted to zero for all curves, and injection start times were aligned. Background sensorgrams were then subtracted from the experimental sensorgrams to yield curves representing specific binding. All of the kinetic data were fit most adequately by assuming a simple bimolecular reaction model for interaction between soluble analyte and immobilized ligand, equivalent to the Langmuir isotherm for adsorption to a surface. For determination of k_{on} only the middle portion of the association curve was used for fitting. For determination of k_{off} only the initial portion of the curve encompassing the fast dissociation phase was used for fitting. The goodness of fit was assessed by inspecting the statistical value χ^2 and the residuals (observed−calculated). The χ^2 values were low (<2) and the residuals randomly distributed about zero. The accuracy of the quantitative measurements of the off rates for the PAP−L3 interactions may be compromised because of the very slow dissociation of the ligand from the protein immobilized on the biosensor chip.

RESULTS AND DISCUSSION

Molecular Model of the PAP−rRNA−L3 Complex and Structure-Based Design of Recombinant PAP Proteins with Altered L3 Binding Affinity. The precise molecular interaction between the ribosomal protein L3 and PAP has yet to be revealed by a crystal structure of the PAP−ribosome complex. However, on the basis of the crystal structure of a large subunit of the *H. marismortui* (HM) ribosome (Protein Data Bank access code 1FFK), the outer surface near residues 65 and 350, which does not interact with rRNA, is the closest region to the α-sarcin/ricin loop. Moreover, on the basis of our previously published molecular model of the PAP−RNA stem loop complex (*15*), half of the active site cleft of PAP is in contact with SRL but the other half which consists of four loop regions, including residues 40−44, 69−70, 91−96 and 120−122, is only partially in contact with SRL and partially exposed to the solvent environment. We reasoned that the partially exposed half of the active site cleft of PAP could be the potential docking site for the L3 molecule. We constructed a molecular model to show the proposed docking position of L3 relative to the active site cleft of PAP. This was accomplished with a docking procedure using a Monte Carlo simulation strategy combined with a docking score evaluation (see Experimental Procedures). Our refined molecular model of the PAP−RNA stem loop complexed with L3 is depicted in Figure 1.

It has been shown that C769T (causing a Pro to Ser change at residue 257) and G765C (causing a Trp to Cys change at residue 255), two adjacent missense mutations of the yeast RPL3 gene which are predicted to structurally alter the encoded L3 protein, significantly affect the programmed −1 ribosomal frame-shift efficiencies of yeast ribosomes (*20*). Interestingly, the mutant protein also showed poor binding to PAP, suggesting that the quaternary structure of a ribosome containing mak8-−1p may differ from a wild-type ribosome such that the binding site for PAP may be masked in the mutant ribosome (*13*). The yeast L3 residues W255 and P257 correspond to the L3 residues W241 and P243 in *H. marismortui* (HM). On the basis of the recently resolved crystal structure of a large ribosomal subunit from HM (Protein Data Bank access code 1FFK) (*16*), these two residues are situated on the nonglobular extension of L3, deeply buried inside the ribosome and interact closely with rRNA reaching toward the peptidyltransferase site (Figure 1A). Therefore, the notion that PAP might interact with these two residues is not consistent with the new structural information provided by the HM crystal structure upon which our model was based.

According to our model, PAP residues 43, 67 (paired with 97), 69, 70, 92, 206−210, 212−213, 217, 224−225, and 253−255 participate in its interaction with rRNA. Our

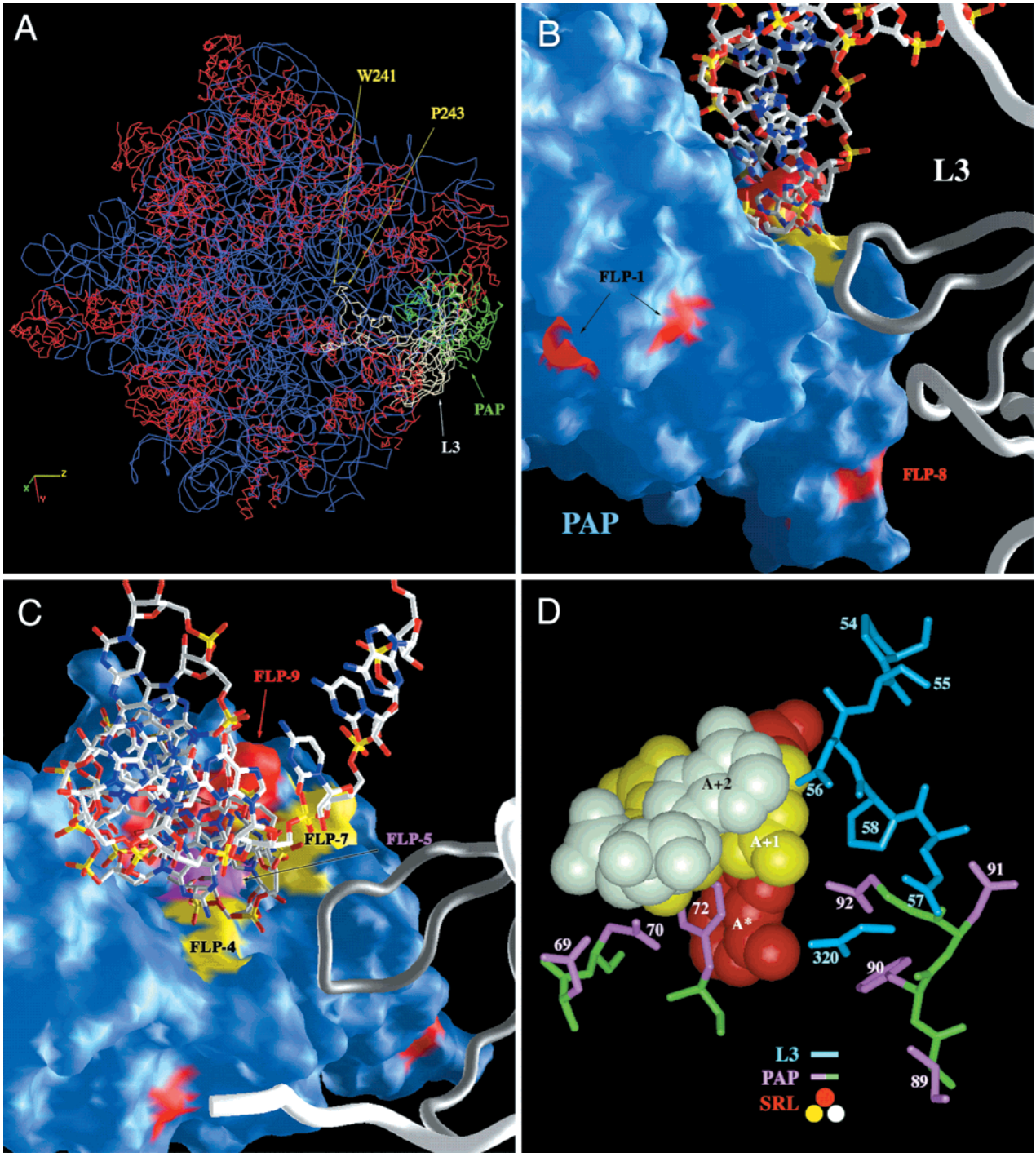

FIGURE 1: Molecular model of PAP interactions with the large ribosome of *Haloarcula marismortui* (HM) and ribosomal protein L3. (A) Model of PAP (green) interacting with the large ribosome unit with rRNA (blue), L3 (white), and the rest of ribosomal proteins (red). As illustrated, the yeast W255 and P257 equivalent residues, W241 and P243, are deeply buried inside the ribosome and interact closely with rRNA reaching toward the peptidyl transferase site. (B and C) PAP−rRNA−L3 model as viewed from two different angles: PAP molecule (blue), L3 (white ribbon), and rRNA (stick model, multicolor). The positions of the alanine-substituted residues of the recombinant PAP mutants FLP-1, FLP-4, FLP-5, FLP-7, and FLP-9 are indicated. The conformation of rRNA (shown in white; phosphate backbone in yellow) was adjusted around the adenine A2697 (A2660 in *E. coli*) of the GAGA tetraloop, and the rest of the PAP molecule remains unchanged. The adenosine was manually adjusted by a 38° rotation at the C5′ position and a 5.4 Å translation of the adenine ring. There are no steric collisions between PAP and nearby ribosomal proteins. L3 is shown as a white ribbon. The loop region around residues 65 and 350 (based on the amino acid sequence of yeast L3) is in close contact with PAP in the regions where mutations occur in FLP-4 and FLP-7 but not in the regions where mutations occur in FLP-1, FLP-5, and FLP-9. The image was created using GRASP software (*23*). (D) Detailed interaction of L3 (blue) with SRL (space-filling model) and PAP (pink and green).

modeling studies indicated that PAP residues 69−70, 90−96, and 118−120 potentially interact with L3. The active center cleft residues Asn^{69}, Asn^{70}, and Asp^{92} as well as the active site residue Arg^{122}, which are not directly involved in the catalytic depurination of rRNA, promote specific interactions with the phosphate backbone of the target SRL of rRNA. On the other hand, these residues are on the protein surface, and all but residue 122 potentially interact with L3 in our model. Therefore, mutations of these residues (except for residue 122) were predicted to result in destabilization

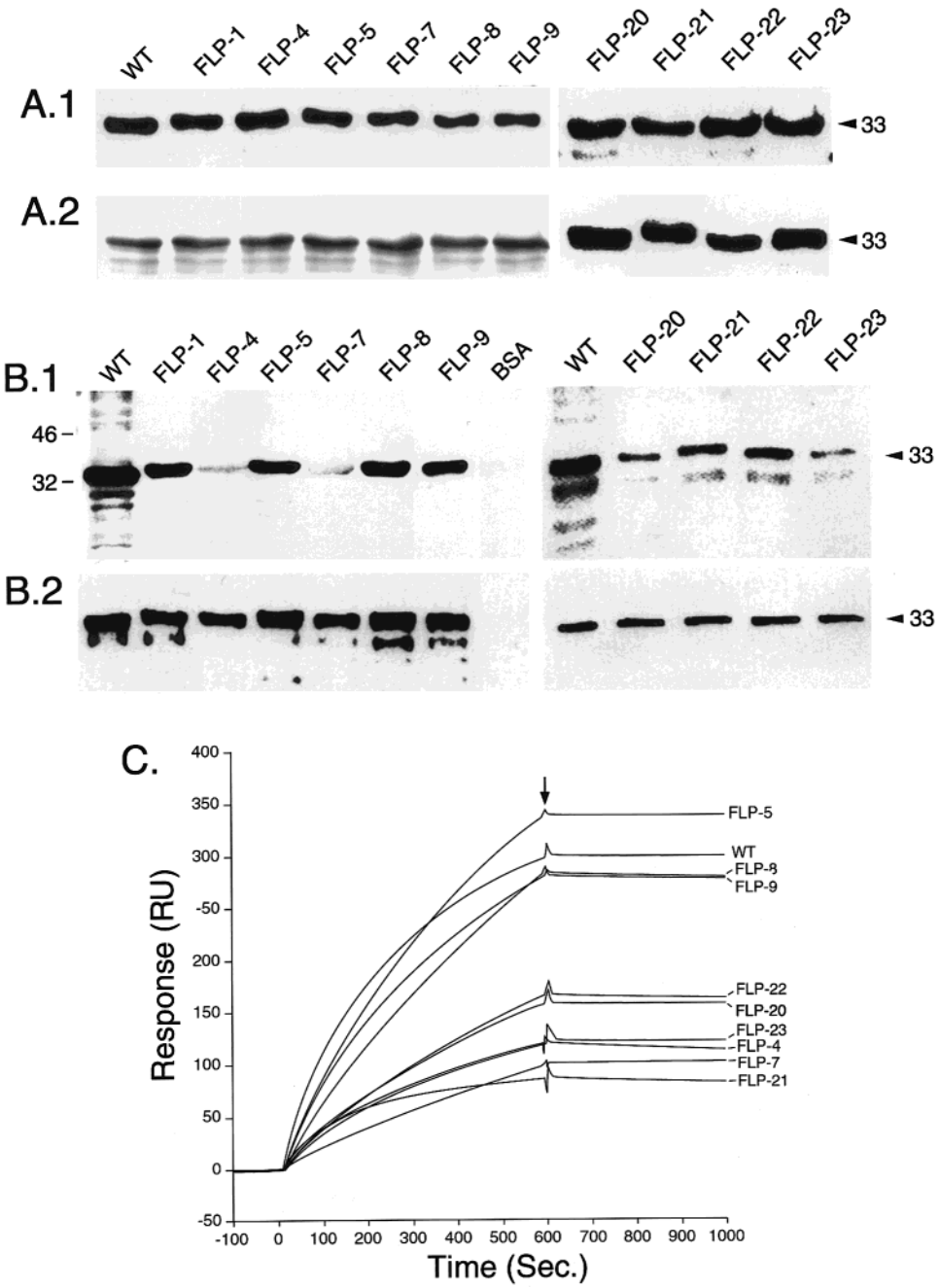

FIGURE 2: (A) Coomassie Blue-stained SDS−12% PAGE (A.1) and Western blot analysis (A.2) of wild-type (WT) and mutant recombinant PAP proteins. The mass of the protein (in kDa) is shown on the right. Each lane contained 5 μg of recombinant PAP protein. (B and C) Association of PAP mutants with ribosomes isolated from rabbit reticulocyte enriched blood. (B.1) Total ribosomal protein (5 μg) was incubated with 1 μg of PAP, and the ribosome−PAP complexes were isolated by ultracentrifugation. The ribosome−PAP complexes were separated through SDS−12% PAGE, electroblotted onto a poly(vinylidene difluoride) (PVDF) membrane, and immunoblotted with a polyclonal antibody to PAP. (B.2) A fraction (5 mL) of the reaction mixture, prior to separation of the PAP−ribosome complex, was removed, separated through SDS−12% PAGE, transferred to PVDF membrane, and immunoblotted with a polyclonal antibody to PAP. The results show that equal amounts of PAP proteins were added to the reaction mixture. (C) Representative sensorgram showing the binding of wild-type and mutant PAP to rabbit ribosomes immobilized on a CM5 sensor chip. Wild-type or mutant PAP proteins were injected onto the surface on which 1200 RU of the MBP−L3 fusion protein had been immobilized at a flow rate of 5 μL/min (40 μL total volume).

of interactions with rRNA and lead to a lower binding affinity with L3. The mutant PAP protein FLP-4 (^{69}AA^{70}) has been engineered by alanine substitution of the active center cleft residues N69 and N70. These residues are located on an antiparallel β turn and interact via hydrogen bonds with the backbone of rRNA from the A +1 position to the A +3 position. Both residues are in close contact with the region near residue 350 on L3 (Figure 1B,C). FLP-7 (^{90}AAA^{92}) has been engineered by alanine substitution of the active center cleft residues 90−92. These residues are positioned on the C-terminal end of the β7 strand and are predicted to contribute to the binding of PAP to the tetraloop structure of RNA. D92 interacts with the base of G(+1). F90 can have van der Waals interactions with four nearby hydrophobic residues. The side chain of residue N91 is located further away from SRL than D92 and has little contact with the tetraloop (Figure 1D). Mutation of F90 is anticipated to affect the local conformation of the β8 strand and the following

Table 1: Kinetic Rates and Dissociation Constants of the Binding Interactions between Recombinant PAP Proteins and Intact Rabbit Ribosomes

mutants	original residue numbered	substituted residue	k_{on} (M^{-1} s^{-1})[a]	k_{off} (M^{-1} s^{-1})[b]	K_D (nM)[c]	K_D/K_D of wild-type PAP
wild type			$8.0 \pm 0.3 \times 10^4$	$2.3 \pm 0.1 \times 10^{-5}$	0.3 ± 0.1	1
FLP-4	^{69}NN^{70}	^{69}AA^{70}	$3.4 \pm 0.1 \times 10^4$	$1.8 \pm 0.1 \times 10^{-4}$	4.7 ± 0.4	16
FLP-5	^{71}LY^{72}	^{71}AA^{72}	$4.8 \pm 0.1 \times 10^4$	$1.1 \pm 0.12 \times 10^{-5}$	0.2 ± 0.1	0.9
FLP-7	^{90}FND^{92}	^{90}AAA^{92}	$1.5 \pm 0.1 \times 10^4$	$1.2 \pm 0.12 \times 10^{-4}$	7.8 ± 0.5	28
FLP-8	^{111}SR^{112}	^{111}AA^{112}	$3.7 \pm 0.3 \times 10^4$	$3.3 \pm 0.13 \times 10^{-5}$	0.9 ± 0.1	3.0
FLP-9	^{122}RY^{123}	^{122}AA^{123}	$8.2 \pm 0.8 \times 10^4$	$6.2 \pm 0.5 \times 10^{-5}$	0.8 ± 0.2	2.7
FLP-20	N69	A69	$2.0 \pm 0.1 \times 10^4$	$1.8 \pm 0.2 \times 10^{-4}$	9.0 ± 0.3	30
FLP-21	F90	A90	$2.3 \pm 0.1 \times 10^4$	$1.2 \pm 0.1 \times 10^{-4}$	5.2 ± 0.4	17
FLP-22	N91	A91	$2.0 \pm 0.1 \times 10^4$	$1.7 \pm 0.1 \times 10^{-4}$	8.5 ± 0.5	28
FLP-23	D92	A92	$3.0 \pm 0.2 \times 10^4$	$2.0 \pm 0.1 \times 10^{-4}$	6.7 ± 0.6	22

[a] k_{on} is the average and SD of measurements from the association phase from two cycles, where 50 nM/150 nM samples were injected. [b] k_{off} is the average and SD of measurements from the dissociation phase from two cycles, where 50 nM/150 nM samples were injected. [c] $K_D = k_{off}/k_{on}$.

loop region which consists of residues 121−123. Mutation of N91 is predicted to have less effect on binding to SRL. Meanwhile, residues 91 and 92 are near residue 58 of a loop region on L3 (see Figure 1D). Residue N91, but not F90 and D92, may interact with this loop region on L3 near residue 65 (Figure 1B,C). Thus mutation of F90 is anticipated to affect the local conformation of the β8 strand and the following loop region which consists of residues 121−123. Taken together, both FLP-4 and FLP-7 were anticipated to show impaired binding of PAP to rRNA and disrupt binding to L3. The single amino acid substitution mutants of PAP, FLP-20 (N69A), FLP-21(F90A), FLP-22 (N91A), and FLP-23 (D92A), were engineered and tested in order to further confirm the importance of the PAP active center cleft residues N69, F90, N91, and D92 for the ability of PAP to bind L3. FLP-24 (N70A) which was also engineered could not be included in biochemical analyses because it was unstable under our solubilization and refolding conditions.

The 121−123 loop of PAP is close enough to interact with the sugar, base, and phosphate groups of the targeted adenosine but is too distant to affect L3 binding. Both Y72 (mutated in FLP-5) and Y123 (mutated in FLP-9) can interact by aromatic group stacking with the base ring of the target adenosine on the basis of the crystal structure of PAP−FMP complex (*21*) and our current model. The side chain of Y123 is partially exposed on the PAP surface, but the side chain of Y72 is mostly buried. Thus Y72 and Y123 are unlikely to interact with L3 although mutations of Y72 and Y123 are predicted to have a significant impact on substrate turnover. Due to the reasons mentioned previously, both FLP-5 (^{71}AA^{72}) and FLP-9 (^{122}AA^{123}) should have unimpaired binding to L3. The control mutants FLP-1 and FLP-8 with alanine substitutions of residues ^{28}KD^{29} and ^{111}SR^{112} that are distant from the active center cleft and are too distant to be interact with L3 on the basis of our model were predicted to exhibit normal L3 binding (Figure 1B,C).

The recombinant PAP mutants with alanine substitutions were constructed using site-directed mutagenesis, as previously described (*15*). These mutant proteins were expressed in the *E. coli* strain, MV1190, as inclusion bodies, purified, solubilized, refolded, and analyzed by SDS−PAGE (Figure 2A). Each of the mutant PAP proteins had an apparent molecular mass of 33 kDa, similar to that of the recombinant wild-type PAP (Figure 2A.1). The refolded recombinant wild-type and mutant proteins were highly immunoreactive with the anti-PAP serum (Figure 2A.2). In a recent study, we demonstrated that the translation inhibition IC_{50} values of the catalytic site mutants FLP-5 (^{71}LY^{72}) and FLP-9 (^{122}AA^{123}), as well as the active center cleft mutants FLP-4 (^{69}AA^{70}) and FLP-7(^{90}AAA^{92}) ,were much higher than those of wild-type PAP (*15*). Furthermore, using a sensitive HPLC method for measuring the amount of adenine released by these mutants from *E. coli* 23/16S rRNA, we determined that wild-yype PAP releases 396 pmol of adenine/μg of RNA, whereas FLP-4 releases only 46 pmol of adenine/μg of RNA and FLP-7 releases only 19 pmol of adenine/μg of RNA (*15*). The ribosome inhibitory activities of the recombinant PAP mutants with alanine substitutions of residues ^{28}KD^{29} and ^{111}SR^{112} that are distant from the catalytic site and active center cleft (FLP-1 and FLP-8), however, were comparable to that of the wild-type PAP (*15*).

Interaction of Wild-Type or Mutant Recombinant PAP Proteins with Rabbit Ribosomes. To evaluate the ability of recombinant PAP proteins to bind ribosomes, intact ribosomes from rabbit reticulocytes were treated with the various PAP proteins, the ribosome−PAP complexes were isolated, and the ribosome-bound PAP proteins were detected by immunoblot analysis using a rabbit anti-PAP antibody. As shown in Figure 2B.1, the active center cleft mutants FLP-4, FLP-7, FLP-20, FLP-21, FLP-22, and FLP-23 showed less binding to intact ribosomes than wild-type PAP. By contrast, all other recombinant PAP proteins, including the catalytic site mutants FLP-5 and FLP-9, bound to the ribosomes as much as wild-type PAP did (Figure 2B.1). Controls confirmed that similar amounts of PAP proteins were used in the respective incubations and immunoprecipitations (Figure 2B.2).

We next compared the binding affinity of recombinant PAP proteins for the intact ribosomes by surface plasmon resonance. The active center cleft mutants FLP-4 and FLP-7 had slower on rates and faster off rates than the wild-yype recombinant PAP protein (Figure 2C, Table 1). The affinities of FLP-4 (K_D = 4.7 nM) and FLP-7 (K_D = 7.8 nM) for the intact rabbit ribosomes were 16-fold and 28-fold lower, respectively, than the affinity of the wild-type PAP (K_D = 0.3 nM) protein (Table 1). The single amino acid mutants of PAP with alanine substitution of the active center cleft residues N69 (FLP-20), F90 (FLP-21), N91 (FLP-22), or D92 (FLP-23) also showed >10-fold reduced ribosome binding, further confirming the importance of the active center cleft for the PAP−ribosome interactions (Table 1). By comparison, the affinity of the catalytic site mutant FLP-5 (K_D = 0.2 nM) was virtually identical to that of wild-type PAP, and the affinity of the other catalytic site mutant FLP-9 (K_D

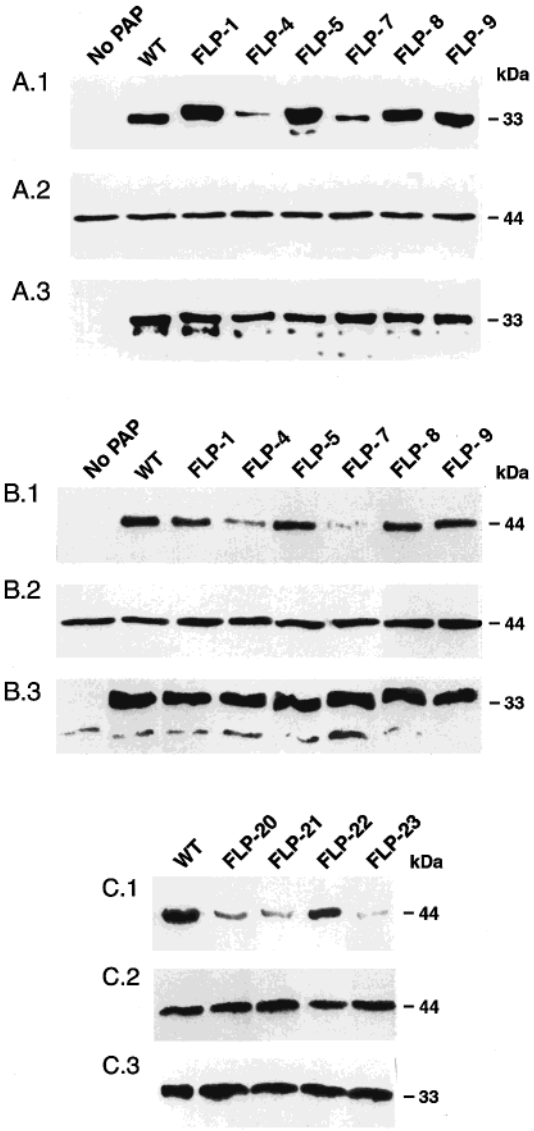

FIGURE 3: Association of wild-type and mutant PAP proteins with in vitro synthesized ribosomal protein L3. (A.1) Coimmunoprecipitated PAP revealed by immunoblotting using anti-PAP antibody. ^{35}S-Labeled L3 was incubated with wild-type and mutant PAP proteins and coimmunoprecipitated with protein A−Sepharose beads precoated with monoclonal antibody to L3. The PAP−L3 complexes were separated through SDS−12% PAGE, transferred to a PVDF membrane, and immunoblotted with a polyclonal anti-PAP antibody. (A.2) The blot was exposed to X-ray film, showing equal amounts of labeled L3 protein in each reaction. (A.3) A fraction (5 μL) of the reaction, prior to the coimmunoprecipitation, was removed from the reaction, separated through SDS−12% PAGE, transferred to a PVDF membrane, and immunoblotted with a polyclonal antibody to PAP. The results show that equal amounts of PAP were added to each reaction. (B.1 and C.1) Coimmunoprecipitated L3 revealed by immunoblotting using anti-L3 antibody. ^{35}S-Labeled L3 was incubated with wild-type and mutant PAP proteins and coimmunoprecipitated with protein A−Sepharose beads precoated with anti-PAP antibody. The PAP−L3 complexes were separated through SDS−12% PAGE, transferred to a PVDF membrane, and immunoblotted with a monoclonal anti-L3 antibody. (B.2 and C.2) A fraction (5 μL) of the reaction, prior to the coimmunoprecipitation, was removed from the reaction, separated through SDS−12% PAGE, dried, and autoradiographed. The results show that equal amounts of labeled L3 protein were added in each reaction. (B.3 and C.3) A fraction (5 μL) of the reaction, prior to the coimmunoprecipitation, was removed from the reaction, separated through SDS−12% PAGE, transferred to a PVDF membrane, and probed with polyclonal antibody to PAP. The results show that equal amounts of PAP were added to each reaction.

= 0.8 nM) was 3-fold lower than that of the wild type. The affinity of mutant FLP-8 (K_D = 0.9 nM), with alanine substitutions of residues ^{111}SR^{112} that are distant from the active center cleft, was only 3-fold lower than that of wild-type PAP (Table 1). Taken together, these results demonstrate that the active center cleft residues are critical for the ribosome binding of PAP.

Interaction of Wild-Type or Mutant Recombinant PAP Proteins with the Ribosome Protein L3. The ribosomal protein L3, a highly conserved protein located at the peptidyltransferase center of the ribosomes, plays a critical role in the binding of PAP to ribosomes and subsequent depurination of the SRL (*13*). Therefore, we next sought to determine if the active center cleft mutants FLP-4, FLP-7, FLP-20, FLP-21, FLP-22, and FLP-23, which exhibited poor binding to intact rabbit ribosomes, can bind L3 protein. To this end, we treated an in vitro synthesized yeast ribosomal protein L3 preparation with various recombinant PAP proteins, immunoprecipitated with a monoclonal anti-L3 antibody, and examined the L3 immune complexes for the presence of any coimmunoprecipitated PAP protein by immunoblotting with a polyclonal anti-PAP antibody. The L3 immune complexes contained relatively less FLP-4 or FLP-7 than other PAP proteins (Figure 3A.1). By comparison, FLP-1, FLP-5, FLP-8, and FLP-9 were coimmunoprecipitated as effectively as wild-type PAP. Controls confirmed that similar amounts of L3 (Figure 4A.2) and mutant PAP proteins (Figure 4A.3) were used in the respective incubations and immunoprecipitations. Similarly, the immune complexes of FLP-4 and FLP-7 contained much less L3 protein than the immune complexes of FLP-1, FLP-5, FLP-8, FLP-9 or wild-type PAP, when the recombinant PAP proteins were immunoprecipitated with the anti-PAP antibody and the coimmunoprecipitation of L3 protein was monitored by immunoblotting with the anti-L3 monoclonal antibody (Figure 3.B1−B3). The poor coimmunoprecipitation of mutant PAP proteins FLP-4 and FLP-7 with the in vitro synthesized yeast L3 protein indicates that the active center cleft residues ^{69}NN^{70} and ^{90}FND^{92} (but not the residues ^{28}KD^{29}, ^{71}LY^{72}, ^{111}SR^{112}, or ^{122}RY^{123} outside the active center cleft) play a pivotal role in L3 binding. The single amino acid substitution mutants FLP-20 (N69A), FLP-21 (F90A), FLP-23 (D92A), and, albeit to a lesser degree, FLP-22 (N91A) also showed reduced L3 binding, which provided further evidence that the active center cleft residues N69, F90, D92, and, to a lesser degree, N91 contribute to the ability of PAP to bind the L3 protein (Figure 3C.1−C.3).

In binding assays using a His-tagged recombinant wild-type PAP protein which was immobilized on the BIAcore sensor chip and surface plasmon resonance technology, which permits direct measurements of the association and disscoation kinetics of binding interactions, recombinant wild-type PAP exhibited high-affinity binding to L3 protein ($k_a = 5.2 \times 10^4$ M^{-1} s^{-1}, $k_d = 4.3 \times 10^{-4}$ s^{-1}, and K_D = 8.2 nM). This binding was blocked by treating the L3 protein with excess soluble recombinant wild-type PAP or excess native PAP, confirming the specificity of the binding interactions (Figure 4).

We next sought to compare the affinity of recombinant PAP proteins for the L3 protein by surface plasmon resonance. In the first series of experiments, we used MBP−L3 protein produced in *E. coli* (Figure 5.A1 and A2). The

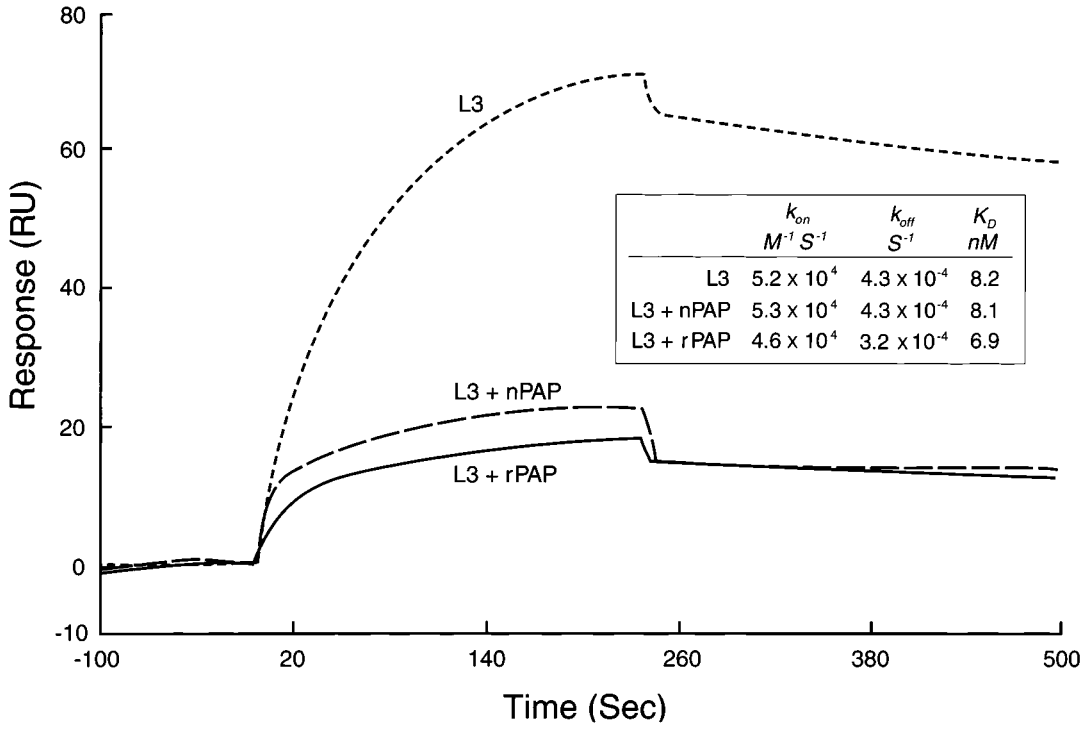

FIGURE 4: Binding specificity of L3 protein to immobilized recombinant wild-type PAP. 6×His−PAP was immobilized onto the NTA-modified surface at a level of 275 RU. A 30 mL solution (25 nM) of MBP−L3 fusion protein was preincubated without or with 250 nM native PAP or recombinant wild-type PAP at room temperature for 1 h and was then injected over immobilized 6×His−PAP at a flow rate of 8 μL/min. Between samples, the binding surface was regenerated by injecting 30 μL of regeneration buffer at a flow rate of 10 μL/min.

Table 2: Kinetic Rates and Dissociation Constants of the Binding Interactions between Recombinant PAP Proteins and Recombinant Yeast Ribosomal Protein L3 (MBP−L3)

mutants	original residue numbered	substituted residue	k_{on} (M^{-1} s^{-1})[a]	k_{off} (M^{-1} s^{-1})[b]	K_D (nM)[c]	K_D/K_D of wild-type PAP
wild type			$3.3 \pm 0.2 \times 10^4$	$8.6 \pm 0.5 \times 10^{-5}$	2.6 ± 0.2	1
FLP-1	^{28}KD^{29}	^{28}AA^{29}	$4.5 \pm 0.3 \times 10^4$	$2.2 \pm 0.1 \times 10^{-4}$	4.7 ± 0.3	1.7
FLP-4	^{69}NN^{70}	^{69}AA^{70}	$3.1 \pm 0.1 \times 10^4$	$4.2 \pm 0.3 \times 10^{-4}$	13.4 ± 0.9	5.2
FLP-5	^{71}LY^{72}	^{71}AA^{72}	$5.3 \pm 0.4 \times 10^4$	$7.9 \pm 0.4 \times 10^{-5}$	1.5 ± 0.1	0.6
FLP-7	^{90}FND^{92}	^{90}AAA^{92}	$2.1 \pm 0.2 \times 10^4$	$2.5 \pm 0.2 \times 10^{-4}$	11.9 ± 0.9	4.6
FLP-9	^{122}RY^{123}	^{122}AA^{123}	$3.7 \pm 0.2 \times 10^4$	$1.1 \pm 0.1 \times 10^{-4}$	3.0 ± 0.2	1.1
FLP-20	N69	A69	$3.4 \pm 0.2 \times 10^4$	$4.4 \pm 0.3 \times 10^{-4}$	12.9 ± 1.1	4.6
FLP-21	F90	A90	$1.7 \pm 0.1 \times 10^4$	$2.6 \pm 0.2 \times 10^{-4}$	15.7 ± 1.3	6.0
FLP-22	N91	A91	$1.4 \pm 0.1 \times 10^4$	$2.5 \pm 0.2 \times 10^{-4}$	17.8 ± 2.0	6.8
FLP-23	D92	A92	$2.5 \pm 0.2 \times 10^4$	$4.3 \pm 0.3 \times 10^{-4}$	17.2 ± 2.0	6.6

[a] k_{on} is the average and SD of measurements from the association phase from two cycles, where 50 nM/150 nM samples were injected. [b] k_{off} is the average and SD of measurements from the dissociation phase from two cycles, where 50 nM/150 nM samples were injected. [c] $K_D = k_{off}/k_{on}$.

MBP protein fused to the N-terminus of the yeast ribosomal protein L3 allowed the L3 protein to be captured in a unique homogeneous orientation on the BIAcore sensor chip. Figure 5.A3 shows a representative sensorgram that was used to generate the kinetic constants summarized in Table 2. The binding traces were analyzed assuming a single bimolecular binding equilibrium between PAP and L3 proteins. The active center cleft mutants FLP-4 and FLP-7 had slower on rates and faster off rates than the wild-type recombinant PAP protein (Table 2, Figure 5.A3). The affinities of FLP-4 (K_D = 13.4 nM) and FLP-7 (K_D = 11.9 nM) for MBP-L3 were approximately 5-fold lower than the affinity of wild-type PAP. The single amino acid substitution mutants FLP-20 (N69A), FLP-21 (F90A), FLP-23 (D92A), and FLP-22 (N91A) also showed a reduced affinity toward L3 binding. Although FLP-22 showed better binding to yeast L3 protein than FLP-20, FLP-21, and FLP-23 (see Figure 3), it did not exhibit a higher affinity than those other active cleft mutants toward the MBP-L3 protein (Table 2). Thus, the MBP tail might affect the binding interactions of L3 with PAP. Nevertheless, the binding affinities of all other recombinant PAP proteins for the MBP−L3 fusion protein were similar to that of wild-yype PAP (Table 2).

Virtually identical results were obtained in binding assays using a His-tagged recombinant L3 protein (6×His−L3) produced in the baculovirus expression system (Table 3, Figure 5.B1−B3). These findings extend the coimmunoprecipitation results and demonstrate the importance of the PAP active cleft residues for the binding interactions between PAP and the ribosomal protein L3. As shown in Figure 5.B4, the high-affinity L3 binding of the catalytic site mutants FLP-5 and FLP-9 confirmed that alanine substitution of the highly conserved catalytic site residues Tyr^{72} and Tyr^{123} does not affect the binding of PAP to the L3 protein, which is in agreement with the assumed role of these residues in binding of PAP to the SRL of rRNA (*20*−*22*).

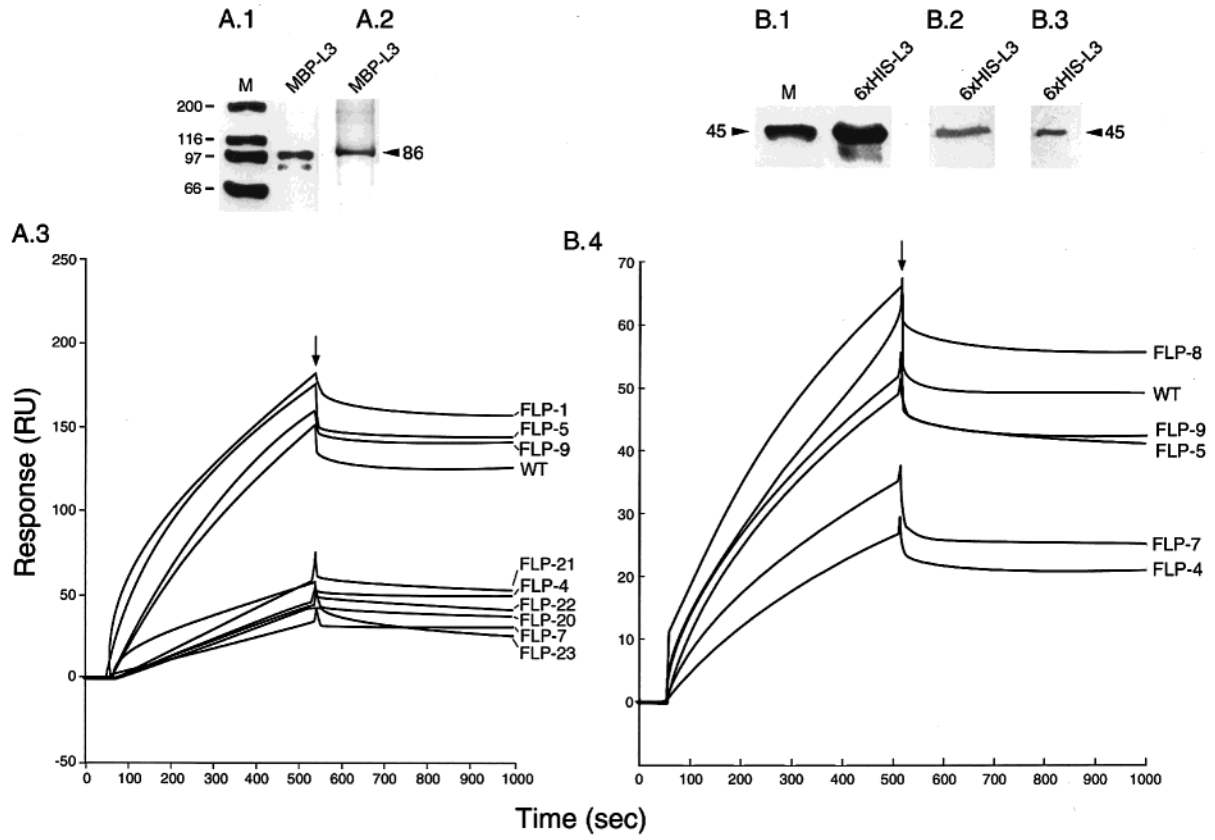

FIGURE 5: Binding of wild-type and mutant PAP proteins to ribosomal protein L3. (A.1) Coomassie Blue-stained SDS−10% PAGE of column-purified recombinant MBP−L3 fusion protein. (A.2) Western blot analysis of MBP−L3 fusion protein using anti-L3 antibody. The mass of the protein (in kDa) is shown on the right. M: molecular mass marker positions (in kDa). (A.3) Representative sensorgram showing the binding of wild-type and mutant PAP proteins to the MBP−L3 fusion protein captured by anti-MBP antibody that was immobilized on a CM5 sensor chip. Wild-type or mutant protein was injected onto the surface on which 1500 RU of the MBP−L3 fusion protein had been immobilized at a flow rate of 5 μL/min (40 μL total volume). The dissociation was started by injecting buffer lacking the sample as indicated by the arrow. (B.1) Coomassie Blue-stained SDS−10% PAGE of column-purified recombinant 6×His−L3 fusion protein. (B.2) Western blot analysis of 6×His−L3 fusion protein using anti-L3 antibody. (B.3) Western blot analysis of 6×His−L3 fusion protein using an anti-His antibody (Qiagen). The mass of the protein (in kDa) is shown on the right. M: molecular mass marker positions (in kDa). (B.4) Representative sensorgram showing the binding of wild-type and mutant PAP to a recombinant yeast ribosomal protein L3 (6×His−L3) biosensor surface.

Table 3: Kinetic Rate and Dissociation Constants of the Binding Interactions between Recombinant PAP Proteins and Recombinant Yeast Ribosomal Protein L3 (MBP−L3)

mutants	original residue numbered	substituted residue	k_{on} (M^{-1} s^{-1})[a]	k_{off} (M^{-1} s^{-1})[b]	K_D (nM)[c]	K_D/K_D of wild-type PAP
wild type			$4.4 \pm 0.4 \times 10^4$	$1.5 \pm 0.18 \times 10^{-4}$	3.5 ± 0.2	1.0
FLP-4	^{69}NN^{70}	^{69}AA^{70}	$4.2 \pm 0.3 \times 10^4$	$7.5 \pm 0.31 \times 10^{-4}$	18.1 ± 0.9	5.2
FLP-5	^{71}LY^{72}	^{71}AA^{72}	$5.0 \pm 0.5 \times 10^4$	$2.3 \pm 0.21 \times 10^{-4}$	4.6 ± 0.3	1.2
FLP-7	^{90}FND^{92}	^{90}AAA^{92}	$4.2 \pm 0.4 \times 10^4$	$5.7 \pm 0.38 \times 10^{-4}$	13.8 ± 0.6	4.0
FLP-8	^{111}SR^{112}	^{111}AA^{112}	$3.4 \pm 0.3 \times 10^4$	$1.2 \pm 0.09 \times 10^{-4}$	3.6 ± 0.3	1.0
FLP-9	^{122}RY^{123}	^{122}AA^{123}	$6.3 \pm 0.5 \times 10^4$	$2.5 \pm 0.17 \times 10^{-4}$	4.0 ± 0.3	1.2

[a] k_{on} is the average and SD of measurements from the association phase from two cycles, where 50 nM/150 nM samples were injected. [b] k_{off} is the average and SD of measurements from the dissociation phase from two cycles, where 50 nM/150 nM samples were injected. [c] $K_D = k_{off}/k_{on}$.

The recombinant PAP protein used in this study contains a 22 amino acid N-terminal signal peptide and a 29 amino acid C-terminal peptide (*15*, *18*). Our previous work demonstrated that the ribosome inhibitory activities of the native and recombinant wild-type protein are comparable (IC_{50} = 0.010 ± 0.004 versus 0.013 ± 0.005 mg/mL) (*18*). Furthermore, our present study shows that native PAP effectively blocks the binding of our recombinant PAP to the L3 protein. Nevertheless, our binding data obtained with the recombinant PAP protein might not accurately reflect the binding of the native protein to the ribosomes in vivo. We are currently trying to cocrystallize native PAP and L3 to decipher the exact structural basis for their interaction. Ultimately, cocrystallization of PAP and a large ribosomal subunit will be required to better understand the in vivo binding of PAP to ribosomes and ribosomal proteins such as L3.

In summary, we employed molecular modeling, structure-based protein design, and site-directed mutagenesis combined with standard immunoprecipitation assays and surface plasmon resonance technology to elucidate the putative role of the PAP active center cleft in the binding of PAP to the ribosomal protein L3, which has been previously shown to mediate the binding of PAP to ribosomes. Our findings provide experimental evidence that the active center cleft of

PAP is important for its binding to ribosomes via the L3 protein and therefore its access to the target α-sarcin/ricin loop of the large ribosomal RNA (rRNA) species in eukaryotic (28S rRNA) and prokaryotic (23S rRNA) ribosomes (*7*, *8*). The insights gained from this study also explain why and how the conserved charged and polar side chains located at the active center cleft of PAP that do not directly participate in the catalytic deadenylation of ribosomal RNA play a critical role in the catalytic removal of the adenine base from target rRNA substrates by affecting the binding interactions between PAP and ribosomes.

The ribosomal protein L3 is expected to bind to and may stabilize the rRNA conformation in which SRL can most effectively bind to and react with PAP. In our model, PAP mutations such as D92A would affect binding with SRL and may thus cause PAP to adopt an unusual binding mode with the tetraloop which consequently changes the docking position of L3. Additionally, L3, rRNA, and PAP are not three separated identities. They form an integrated complex sharing an overlapped binding region. Interaction between two componets of this complex would affect their interaction with the third component. Therefore, under physiologic conditions, L3 may have reduced binding affinity to the PAP mutants which have impaired binding with SRL. We postulate that the active center cleft mutants would have markedly reduced ability to interact with the L3 ribosomal protein under physiologic conditions because of their poor L3 binding as well as poor rRNA binding.

Our results showing the ability of PAP to bind purified L3 in the absence of other ribosomal components indicate that conformational changes of L3, if any should occur as a result of its incorporation into the ribosome, are not required for its interactions with PAP. Therefore, our model for L3−PAP interactions did not take into account any conformational changes which may occur when L3 is incorporated into the ribosome. The elucidation of the exact details of the physical interactions between L3 and PAP will require the cocrystallization of these two proteins and ideally the cocrystallization of a large ribosomal subunit and PAP.

ACKNOWLEDGMENT

We thank Tammy J. Denton, Dawn M. Dahlke, Michelle L. Henning, Rebecca S. Larue, Dina Clementson, Brad Nodland, and Andrea Dopkins for technical assistance.

REFERENCES

1. Irvin, J. D. (1995) Antiviral proteins from Phytolacca, *Antiviral Proteins in Higher Plants* (Chessin, M., DeBorde, D., and Zipf, A., Eds.) CRC Press, Boca Raton, FL.
2. Irvin, J. D. (1983) *Pharmacol. Ther. 21*, 371−387.
3. Irvin, J. D., and Uckun, F. M. (1992) *Pharmacol. Ther.* 55, 279−302.
4. Uckun, F. M. (1993) *Br. J. Haematol. 85*, 435−438.
5. Uckun, F. M., and Reaman, G. H. (1995) *Leuk. Lymphoma 18*, 195−201.
6. Myers, D. E., and Uckun, F. M. (1995) *Leuk. Lymphoma 18*, 119−122.
7. Endo, Y., Mitsui, K., Motizuki, M., and Tsurugi, K. (1987) *J. Biol. Chem. 262*, 5908−5912.
8. Endo, Y., and Tsurugi, K. (1988) *J. Biol. Chem. 263*, 8735−8739.
9. Obrig, T. G., Irvin, J. D., and Hardesty, B. (1973) *Arch. Biochem. Biophys. 155*, 278−289.
10. Gessner, S. L., and Irvin, J. D. (1980) *J. Biol. Chem. 255*, 3251−3253.
11. Montanaro, L., Sperti, S., Mattioli, A., Testoni, G., and Stirpe, F. (1975) *Biochem. J. 146*, 127−131.
12. Barbieri, L., Battelli, M. G., and Stirpe, F. (1993) *Biochim. Biophys. Acta 1154*, 237−282.
13. Hudak, K. A., Dinman, J. D., and Tumer, N. E. (1999) *J. Biol. Chem. 274*, 3859−3864.
14. Uchiumi, T., Sato, N., Wada, A., and Hachimori, A. (1999) *J. Biol. Chem. 274*, 681−686.
15. Rajamohan, F., Pugmire, M. J., Kurinov, I. V., and Uckun, F. M. (2000) *J. Biol. Chem. 275*, 3382−3390.
16. Ban, N., Nissen, P., Hansen, J., Moore, P. B., and Steitz, T. A. (2000) *Science 289*, 905−920.
17. Sack, J. S. (1988) *J. Mol. Graphics 6*, 244−249.
18. Rajamohan, F., Engstrom, C. R., Denton, T. J., Engen, L. A., Kourinov, I., and Uckun, F. M. (1999) *Protein Expression Purif. 16*, 359−368.
19. Boyd Hardesty, W. M., and Culp, W. (1979) *Methods Enzymol. 33*, 316−327.
20. Peltz, S. W., Hammell, A. B., Cui, Y., Yasenchak, J., Puljanowski, L., and Dinman, J. D. (1999) *Mol. Cell. Biol. 19*, 384−391.
21. Monzingo, A. F., Collins, E. J., Ernst, S. R., Irvin, J. D., and Robertus, J. D. (1993) *J. Mol. Biol. 233*, 705−715.
22. Poyet, J. L., Hoeveler, A., and Jongeneel, C. V. (1998) *Biochem. Biophys. Res. Commun. 253*, 582−587.
23. Nicholls, A., Sharp, K. A., and Honig, B. (1991) *Proteins 11*, 281−296.

BI002851P